Magnon valve effect and resonant transmission in a one-dimensional magnonic crystal

Y. W. Xing,[1,2,*] Z. R. Yan,[1,*] and X. F. Han[1,2,3,†]

[1]*Beijing National Laboratory for Condensed Matter Physics, Institute of Physics, University of Chinese Academy of Sciences, Chinese Academy of Sciences, Beijing 100190, China*

[2]*Center of Materials Science and Optoelectronics Engineering, University of Chinese Academy of Sciences, Beijing 100049, China*

[3]*Songshan Lake Materials Laboratory, Dongguan, Guangdong 523808, China*

(Received 10 November 2020; revised 11 December 2020; accepted 4 February 2021; published 18 February 2021)

We theoretically investigate the transmission of exchange-dominated spin waves in a one-dimensional magnonic crystal (MC) with a periodic exchange bias field. By recasting the Landau-Lifshitz-Gilbert equation into an effective Schrödinger equation and establishing spin-wave functions, it is found that MCs with upward (up) and downward (down) magnetization, respectively, correspond to the rectangular *N*-fold barriers and wells for magnons. The broadband transmission spectra in up and down states are systematically investigated. We show the phenomena of the magnon resonant transmission in both states and calculate the resonant transmission wave functions, which are related to the magnon density. Our results also show a transmission spectra shift effect (TSSE) between up and down states, which is found to be general in this system. Furthermore, the TSSE is useful to design a type of magnon valve, the magnonic-crystal-based magnon valve (MCMV), which has a large on/off ratio and bandwidth. By high-throughput screening, 125 000 groups of parameters of the MC are calculated, and 1948 parameter groups of high-performance MCMVs are screened out. Our work clarifies the physical details of the exchange-dominated spin-wave transmission in rectangular *N*-fold barriers and wells and also provides a promising route for designing novel magnonic devices.

DOI: 10.1103/PhysRevB.103.054425

I. INTRODUCTION

Spin waves, the elementary excitation of the magnetic system, were first introduced by Bloch 91 years ago [1]. After that, Holstein and Primakoff [2] and Dyson [3] introduced spin-wave quanta which are called magnons. Each quantized magnon carries a spin angular momentum of $-\hbar$ and is regarded as a potential information carrier. Magnonics is the research field encompassing the transmission, storage, and processing of information by using magnons [4–8]. In magnonics, the manipulation of the magnon transmission is an important branch due to its potential application in magnonic devices [9–17]. One of the effective ways to manipulate magnon transmission is injecting spin waves into the magnonic crystals (MCs).

As early as 1976, Sykes *et al.* experimentally studied the spin-wave propagation in a periodic structure [18], which is regarded as the first work on MCs [19], and the concept of MCs was first introduced by Nikitov *et al.* in 2001 [20]. MCs, as the magnetic analog of photonic and sonic crystals, are artificial mesoscopic media with periodic lateral variations in magnetic properties [6,7,19,21]. The spectra of magnons in such media, significantly different from those in uniform media, have band structures containing band gaps, where propagations of spin waves are prohibited [6,7,19,21]. The experimental works of MCs mainly focus on the dipole-dominated spin waves [12,18,22–24]. These types of MCs are usually in micron or millimeter scales, and their frequency ranges are mainly 1–10 GHz, which will limit the reduction of the device sizes and the information processing speed. Therefore, it is necessary to investigate the exchange-dominated spin waves with short wavelengths ($\lambda < 100$ nm) in MCs, and we contribute to this field in this paper.

In this work, we construct a model for a one-dimensional MC with a periodic exchange bias (EB) field. It is found that the MCs with upward (up) and downward (down) magnetization correspond to the rectangular *N*-fold barriers and wells for exchange-dominated spin waves, respectively. Via the transfer matrix method (TMM) [25,26], the transmission coefficients in up and down states are investigated, and the phenomena of the magnon resonant transmission are found. Our results also show that a transmission spectra shift effect (TSSE) leads to the different transmission coefficients in up and down states. Based on the TSSE, a type of magnon valve called a magnonic-crystal-based magnon valve (MCMV) with high performance for manipulating the magnon transmission is proposed. Through the high-throughput screening method, plenty of MCMVs with large on/off ratios and bandwidths are screened out. Our work can serve as a promising tool for investigating the exchange-dominated spin-wave transmission and also provides guidance for future magnonic devices.

II. ANALYTICAL MODEL

In magnetic films, the dynamics of spin-wave propagation (magnon transmission) is governed by the Landau-Lifshitz-

*These authors contributed equally to this work.
†xfhan@iphy.ac.cn

Gilbert (LLG) equation

$$\frac{\partial \mathbf{m}}{\partial t} = -\gamma\mu_0 \mathbf{m} \times \mathbf{H}_{\text{eff}} + \alpha \mathbf{m} \times \frac{\partial \mathbf{m}}{\partial t}, \tag{1}$$

where $\mathbf{m} = \mathbf{M}/M_s$ is the unit magnetization vector with the saturation magnetization M_s, $\gamma = 1.76 \times 10^{11}$ rad/(s T) is the gyromagnetic ratio, and α is the Gilbert damping coefficient. Generally, the effective field $\mathbf{H}_{\text{eff}}$, including the exchange field $\mathbf{H}_{\text{ex}}$, dipolar field $\mathbf{H}_{\text{d}}$, anisotropy field $\mathbf{H}_{\text{a}}$, and external field $\mathbf{H}_{\text{ext}}$, has the form $\mathbf{H}_{\text{eff}} = \mathbf{H}_{\text{ex}} + \mathbf{H}_{\text{d}} + \mathbf{H}_{\text{a}} + \mathbf{H}_{\text{ext}}$. For the case of magnetization perpendicular to the films, the spin-wave dispersion relation is given by [27]

$$\omega^2 = [A^* k^2 + \omega_H][A^* k^2 + \omega_H + \omega_M f(kd)], \tag{2}$$

where $A^* = 2\gamma A/M_s$, with A being the exchange constant; k is the magnitude of the wave vector; $\omega_H = \gamma\mu_0(H_a + H_{ext})$, with H_a and H_{ext} being the magnitudes of the anisotropy field and external field, respectively; and d is the thickness of the magnetic film. Here, H_a represents the effective anisotropy field which includes the influence of the demagnetization field. $\omega_M = \gamma\mu_0 M_s$ and $f(kd) = 1 - [1 - \exp(-kd)]/kd$ are terms which show the influence of the dipole-diploe interaction for a perpendicularly magnetized film. As reported by Lenk *et al.* [28], for cases in which the spin waves propagate in the films with in-plane magnetization, when k is over 0.0628 rad/nm (or wavelength λ is below 100 nm), the spin-wave dispersion is dominated by the exchange interaction, and the dipolar influence can be ignored. By calculation, we found that the perpendicular case is similar to the in-plane cases because the dipolar term can also be ignored when k is high enough. Thus, the exchange-dominated spin-wave dispersion relation is written as [29,30]

$$\omega = A^* k^2 + \omega_H. \tag{3}$$

We consider the transmission of the exchange-dominated spin waves in a one-dimensional MC with periodic EB field. Figures 1(a) and 1(b) show the side views of this MC in up and down states, respectively. The blue rectangles represent the ferromagnet (FM) with perpendicular magnetic anisotropy (PMA), such as PMA CoFeB [31,32]. The periodic green rectangles on top of the FM represent the antiferromagnets (AFMs) with perpendicular EB, such as MnN [32]. The number of periodic AFMs, the width of each AFM, and the distance between two adjacent AFMs are described by N, a, and b, respectively. The direction of the EB field $\mathbf{H}_{\text{eb}}$ is fixed upward. The magnetization state of the FM is up and down in Figs. 1(a) and 1(b), respectively. In this paper, the external field $H_{\text{ext}} = 0$ because we consider a large PMA for which the stable up and down states can be constructed under zero external field. The parameters of the MC used for calculations are the following: saturation magnetization $M_s = 1.1 \times 10^6$ A/m [33], exchange constant $A = 1.1 \times 10^{-11}$ J/m [33], PMA field $H_a = 3000$ Oe [32], and perpendicular EB field $H_{\text{eb}} = 2000$ Oe [32]. The frequency of spin waves is high enough ($\omega/2\pi > 20$ GHz, $\lambda < 60.74$ nm) to ensure that the spin waves are exchange dominated, which is discussed in detail in the Supplemental Material [34], Sec. I.

The transmission coefficients in this MC are derived below. The unit magnetization is assumed to be $\mathbf{m} = m_x\hat{x} + m_y\hat{y} + m_z\hat{z}$, with $m_{x,y} \ll 1$ and $m_z \approx 1$. By defining a spin-wave function $\psi = m_x - im_y$ and neglecting the damping, the LLG equation (1) can be recast into an effective Schrödinger equation [29,30,35–39],

$$i\hbar\frac{\partial \psi}{\partial t} = \left(\frac{\hat{p}^2}{2m^*} + V\right)\psi, \tag{4}$$

where $\hat{p} = -i\hbar\nabla$ is the momentum operator and $m^* = \hbar/2A^*$ is the effective mass of magnons. V represents the potential energy and has different expressions depending on the regions of the MC. In the regions without AFMs, $V = V_0 = \hbar\gamma\mu_0 H_a$, with H_a being the PMA field. In contrast, in the regions with AFMs, $V = \hbar\gamma\mu_0(H_a \pm H_{eb})$, with H_{eb} being the EB field, where $\pm$ corresponds to the cases with N-fold barriers (+) and N-fold wells (−), as shown in Figs. 1(a) and 1(b). For

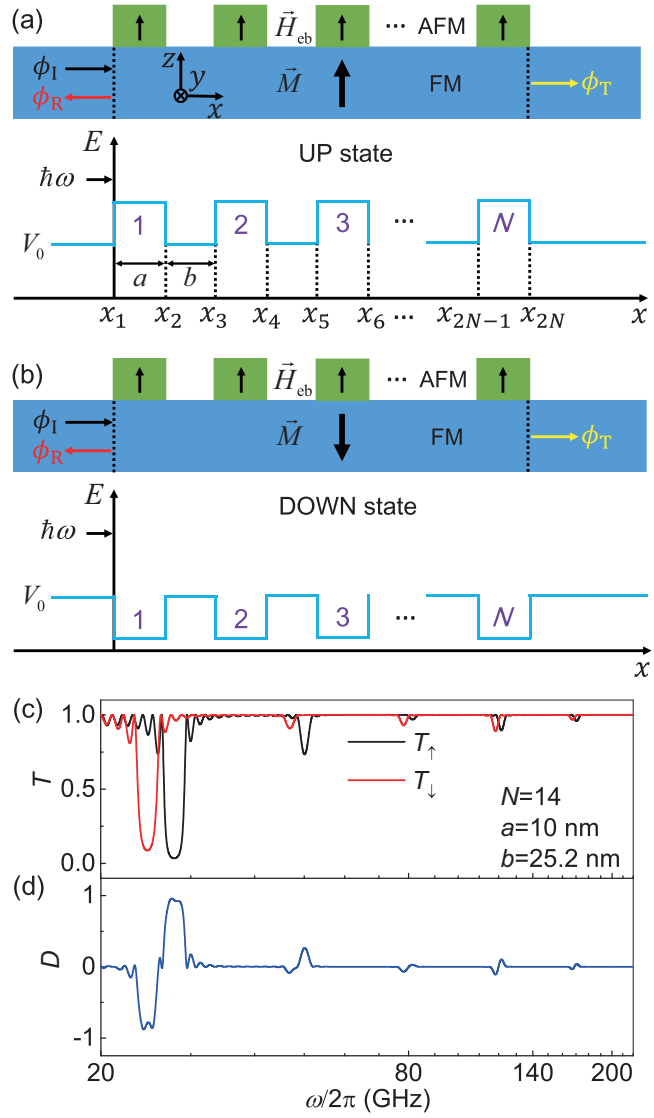

FIG. 1. The magnon transmission in a one-dimensional MC. The schematic diagrams of the MC in (a) the up state and (b) the down state. (c) The broadband transmission spectra in up and down states, corresponding to the black curve ($T_\uparrow$) and red curve ($T_\downarrow$) respectively. The parameters of the MC are the following: $N = 14$, $a = 10$ nm, and $b = 25.2$ nm. (d) The difference between $T_\uparrow$ and $T_\downarrow$ as a function of $\omega/2\pi$. $\omega/2\pi$ is shown in logarithm scale.

simplicity, we define a normalized wave function $\hat{\psi}(x,t) = \psi(x,t)/a_{\rm I}$, where $a_{\rm I} = |\psi_{\rm I}(x,t)|$ represents the amplitude of the incident waves. By separating the space-dependent and time-dependent functions via $\hat{\psi}(x,t) = \phi(x)T(t)$, with $T(t) = e^{-i\omega t}$, the Schrödinger equation (4) turns into a stationary Schrödinger equation. The theoretical task in this work is to solve the stationary Schrödinger equation in the case of N-fold barriers and wells. The MC is divided into $2N+1$ regions by the N-fold barriers (wells); $j = 1, 2, \ldots, N$ represent the jth barrier (well), while $s = 1, 2, 3, \ldots, 2N, 2N+1$ represent the sth region. According to Eq. (3), the expressions for the wave vectors in different regions are

$$\begin{aligned} k_s = k &= \sqrt{\frac{M_{\rm s}}{2\gamma A}(\omega - \gamma\mu_0 H_{\rm a})} \\ &\quad s = 1, 3, 5, \ldots, 2N+1, \\ k_s = k_{b(w)} &= \sqrt{\frac{M_{\rm s}}{2\gamma A}[\omega - \gamma\mu_0(H_{\rm a} \pm H_{\rm eb})]} \\ &\quad s = 2, 4, 6, \ldots, 2N, \end{aligned} \tag{5}$$

where $+$ is for $k_{\rm b}$ in the barrier regions and $-$ is for $k_{\rm w}$ in the well regions. For the jth barrier (well), the left boundary conditions at x_{2j-1} are written as [25,30]

$$\begin{aligned} \phi_{2j-1}(x_{2j-1}) &= \phi_{2j}(x_{2j-1}), \\ \left.\frac{d\phi_{2j-1}}{dx}\right|_{x=x_{2j-1}} &= \left.\frac{d\phi_{2j}}{dx}\right|_{x=x_{2j-1}}. \end{aligned} \tag{6}$$

The right boundary conditions at x_{2j} are

$$\begin{aligned} \phi_{2j}(x_{2j}) &= \phi_{2j+1}(x_{2j}), \\ \left.\frac{d\phi_{2j}}{dx}\right|_{x=x_{2j}} &= \left.\frac{d\phi_{2j+1}}{dx}\right|_{x=x_{2j}}. \end{aligned} \tag{7}$$

The waves in regions 1–$(2N+1)$ are assumed to be $\phi_s(x) = A_s e^{ik_s x} + B_s e^{-ik_s x}$. The incident and reflected waves in region 1 and the transmitted waves in region $2N+1$ are assumed to be

$$\phi_1(x) = \phi_{\rm I}(x) + \phi_{\rm R}(x) = e^{ikx} + re^{-ikx}, \tag{8}$$

$$\phi_{2N+1}(x) = \phi_{\rm T}(x) = te^{ikx}. \tag{9}$$

The numerical solutions of the reflection coefficients $R = |r|^2$ and transmission coefficients $T = |t|^2$ can be obtained through the TMM [25,26].

III. RESULTS AND DISCUSSION

In Fig. 1(c), $T_\uparrow$ ($T_\downarrow$) shows the magnon transmission coefficients in the up (down) state. The main characteristic of the transmission spectra is the band structure with periodic valleys and peaks, which are similar to the transmission spectra reported in previous works [12,18,20,22–24,40]. The deep valleys of $T_\uparrow$ and $T_\downarrow$ show the strong reflection of magnons, while the peaks where $T_\uparrow = 1$ (or $T_\downarrow = 1$) represent the magnon resonant transmission. The tendencies of $T_\uparrow$ and $T_\downarrow$ are very similar. However, the positions of their valleys and resonant peaks are different. It seems that $T_\downarrow$ can be regarded as $T_\uparrow$ shifted to a lower frequency. This transmission spectra shift (TSS) can lead to a significant difference between $T_\uparrow$ and $T_\downarrow$. Thus, we define a parameter called D to characterize the difference in transmission coefficients between up and down states:

$$D(\omega) = T_\downarrow(\omega) - T_\uparrow(\omega). \tag{10}$$

Figure 1(d) shows the transmission difference in $T_\uparrow$ and $T_\downarrow$ from Fig. 1(c). When $\omega/2\pi$ is between about 24.0 and 25.4 GHz, $T_\uparrow$ oscillates around 0.9, and $T_\downarrow$ is around 0.1; thus, D is below -0.78. This value indicates that the up state provides high transmission for magnons, while the down state leads to strong reflection. In contrast, when $\omega/2\pi$ is between about 27.1 and 28.7 GHz, D is above 0.87, showing a reverse transmission behavior of magnons in up and down states. This behavior demonstrates that the proposed MC can be used as a magnon valve because the magnon transmission depends on the magnetization state of the FM, i.e., up and down states. This magnon valve is similar to giant magnetoresistance (GMR)-based spin valves [41,42], tunnel magnetoresistance (TMR)-based magnetic tunnel junctions (MTJs) [43–49], and magnon-valve-effect-based magnon valves [13] and magnon junctions [14]. Therefore, this proposed MC can be called a MCMV. Obviously, D, which indicates the on/off ratio of the magnon transmission, is the key parameter for the MCMV. The optimization of D will be discussed in the last part of this paper.

Next, the physical details of the magnon resonant transmission in this MC are investigated. As seen in Fig. 1(c), a large value of N causes numerous and complex resonant peaks, which makes it difficult to analyze the crucial points. Therefore, a smaller N is chosen for further discussion. Figure 2(a) shows $T_\uparrow$ and $T_\downarrow$ at $N = 1$ and $a = 10$ nm. The details are shown in Fig. 2(b) by enlarging Fig. 2(a). The tendencies of $T_\uparrow$ and $T_\downarrow$ are similar to those in Fig. 1(c), although the numbers of resonant peaks are different. The TSS between $T_\uparrow$ and $T_\downarrow$ still exists, which suggests it is independent of N, a, and b. Figure 2(b) shows four resonant peaks marked E_1–E_4, which represent the resonant transmission energy levels (RTELs). Figures 2(c)–2(f) show the moduli of the resonant transmission wave functions (RTWFs) $|\Phi_n(x)|$ of the up state with $n = 1$–4, respectively. The red lines represent $|\Phi_n(x)|$ in the regions without the barrier, while the blue lines represent $|\Phi_n(x)|$ in the barrier regions. According to the definition of the spin-wave function, $|\Phi_n(x)| = \sqrt{|m_x(x)|^2 + |m_y(x)|^2}/a_{\rm I}$ also represents the distribution of the magnon density. All $|\Phi_n(x)|$ are space symmetric and consist of numbers of peaks. It is easy to understand the symmetry because the transmission from left to right is the same as that from right to left in the resonant cases. The number of peaks in $|\Phi_n(x)|$ increases as n is increased, which indicates that the distribution of the magnon density become more complex as E_n increases to a higher level. For $N = 2$, 3, 5, the RTELs and RTWFs are also investigated and are shown in the Supplemental Material [34], Sec. II. As N is increased to infinity, the pass bands and forbidden bands start to appear in the transmission spectra, and this result is shown in the Supplemental Material [34], Sec. III.

The results for $T_\uparrow$ and $T_\downarrow$ become different when the values of N, a, and b change. Nevertheless, the main results are

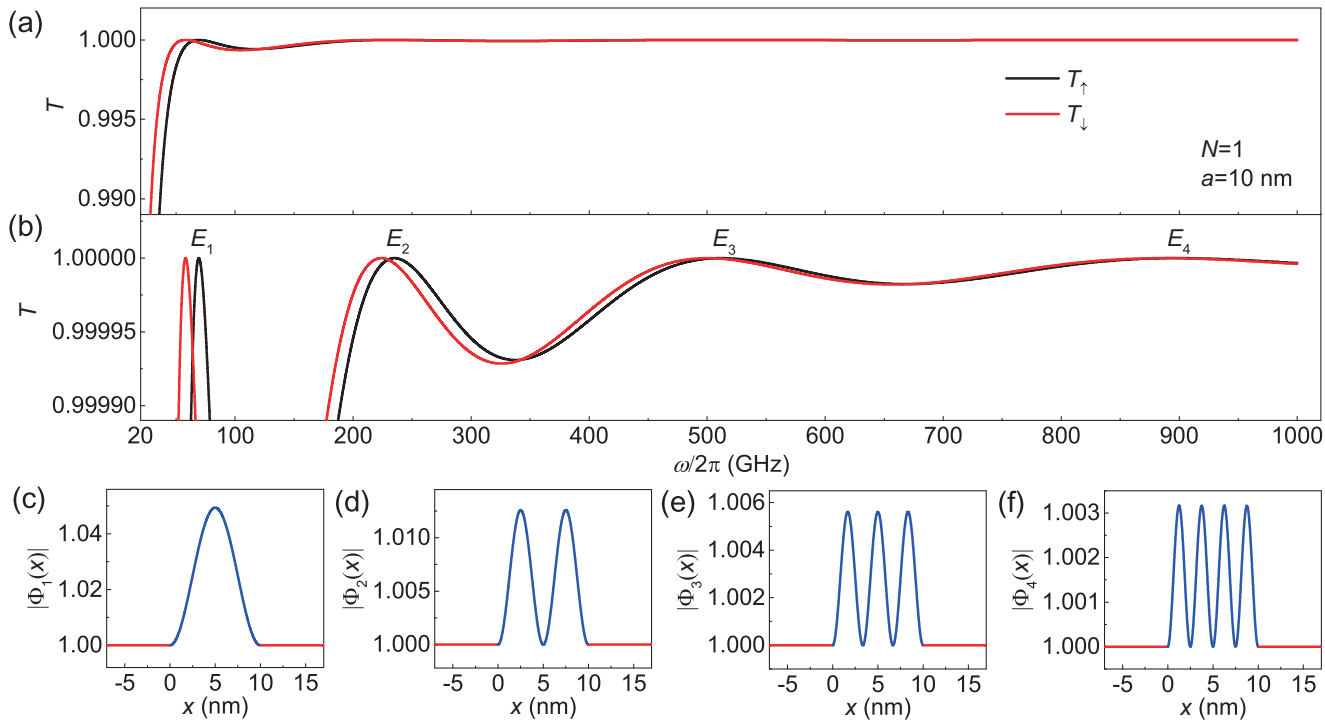

FIG. 2. The magnon transmission spectra and RTWFs at $N = 1$ and $a = 10$ nm. (a) The transmission spectra in up and down states. (b) The details of the transmission spectra in (a). E_1–E_4 represent the RTELs. (c)–(f) The moduli of the RTWFs $|\Phi_n(x)|$ (n = 1–4) corresponding to E_n (n = 1–4) of the up state, which also suggest the distribution of the magnon density in the resonant cases. In (c)–(f), the red lines represent $|\Phi_n(x)|$ in the regions without the barrier, while the blue lines represent the regions with the barrier.

similar to Fig. 2. There are two characteristics which are independent of N, a, and b. First, the phenomenon of the magnon resonant transmission always exists, showing that only magnons with a specific frequency are allowed to totally pass through the MC. A similar phenomenon was reported in photonic crystals [50]. Second, the TSS between $T_\uparrow$ and $T_\downarrow$ is a general phenomenon. For $N = 1$, the frequency shift of the corresponding resonant peaks between $T_\uparrow$ and $T_\downarrow$ can be analytically proved to be $\Delta\omega = -2\gamma\mu_0 H_{\rm eb}$ as follows. The transmission problem of a single barrier is well known, and the transmission coefficient $T_\uparrow$ is given by

$$T_\uparrow = \left[1 + \frac{1}{4}\left(\frac{k}{k_{\rm b}} - \frac{k_{\rm b}}{k}\right)^2 \sin^2(k_{\rm b}a)\right]^{-1}. \tag{11}$$

The derivation details of Eq. (11) are given in the Supplemental Material [34], Sec. IV. It is obvious that the condition of the resonant transmission is $\sin(k_{\rm b}a) = 0$; in other words, $k_{\rm b}a = n\pi$ ($n = 1, 2, 3, \ldots$). By uniting the resonant condition with Eq. (3), the nth resonant frequency is written as

$$\omega_\uparrow^n = A^*\left(\frac{n\pi}{a}\right)^2 + \gamma\mu_0(H_{\rm a} + H_{\rm eb}). \tag{12}$$

Similarly, for the case of a single well, the transmission coefficient $T_\downarrow$ is given by

$$T_\downarrow = \left[1 + \frac{1}{4}\left(\frac{k}{k_{\rm w}} - \frac{k_{\rm w}}{k}\right)^2 \sin^2(k_{\rm w}a)\right]^{-1}. \tag{13}$$

The derivation details of Eq. (13) are also given in the Supplemental Material [34], Sec. IV. The condition of the resonant transmission is $k_{\rm w}a = n\pi$ ($n = 1, 2, 3, \ldots$), and the nth resonant frequency is written as

$$\omega_\downarrow^n = A^*\left(\frac{n\pi}{a}\right)^2 + \gamma\mu_0(H_{\rm a} - H_{\rm eb}). \tag{14}$$

Uniting Eq. (12) with Eq. (14), the shift of the nth resonant peaks between $T_\uparrow$ and $T_\downarrow$ can be given by

$$\Delta\omega = \omega_\downarrow^n - \omega_\uparrow^n = -2\gamma\mu_0 H_{\rm eb}. \tag{15}$$

Equation (15) shows that the relative distance of the corresponding peaks of $T_\uparrow$ and $T_\downarrow$ are constant, which leads to a TSS between $T_\uparrow$ and $T_\downarrow$. It also demonstrates that the EB field $H_{\rm eb}$ plays an important role in the TSS. For $N \geqslant 2$, it is hard to analyze the shift of the resonant peaks with those complex analytical expressions. Fortunately, one can always see the TSS with the numerical results shown in Figs. 1(c), 2(b) and 3 and Figs. 2–4 in the Supplemental Material. Based on these proofs, we conclude that the TSS is general in the system of N-fold barriers and wells, which is thus named a TSSE.

Figures 3(a)–3(c) show the influence of the periodic number N on the transmission coefficients $T_\uparrow$ and $T_\downarrow$ and the transmission difference D. First, the number of resonant peaks increases with the increase of N, showing that the number of resonant transmission states increases. Second, the valleys of $T_\uparrow$ and $T_\downarrow$ become deeper as N increases. This increasing deepness can be explained by the mechanism in which as the number of the barriers or wells increases, the reflection of magnons become stronger, which leads to smaller $T_\uparrow$ and $T_\downarrow$. Figures 3(c)–3(e) demonstrate the influence of the PMA

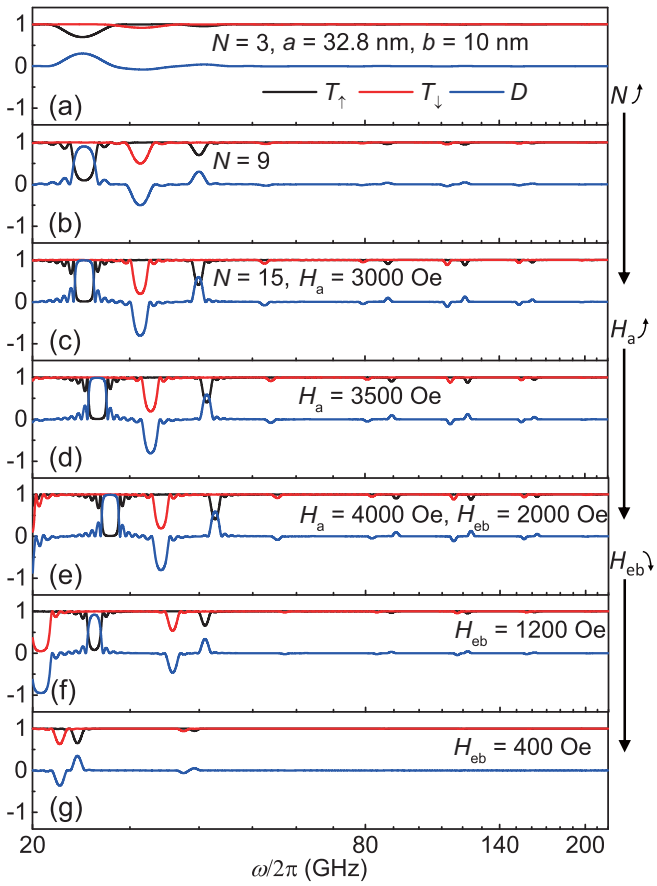

FIG. 3. The influences of N, H_a, and H_{eb} on $T_\uparrow$ (black), $T_\downarrow$ (red), and D (blue). The influence of (a)–(c) increasing N, (c)–(e) increasing H_a, and (e)–(g) decreasing H_{eb}. $\omega/2\pi$ is shown in logarithm scale.

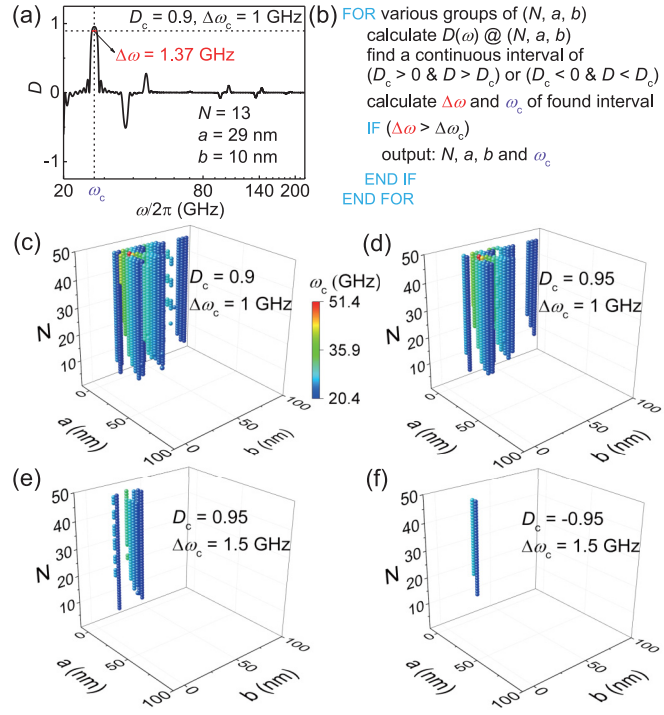

FIG. 4. High-throughput screening results of (N, a, b) for high D_c and large $\Delta\omega_c$. (a) The schematic diagram of D_c, $\Delta\omega_c$, $\Delta\omega$, and ω_c. $\omega/2\pi$ is shown in logarithm scale. (b) The pseudocode of the high-throughput algorithm. The screening results of N, a, and b at (c) $D_c = 0.9$, $\Delta\omega_c = 1$ GHz, (d) $D_c = 0.95$, $\Delta\omega_c = 1$ GHz, (e) $D_c = 0.95$, $\Delta\omega_c = 1.5$ GHz, and (f) $D_c = -0.95$, $\Delta\omega_c = 1.5$ GHz. The color bars in (c)–(f) are the same and are defined to the right of (c).

field H_a. It is obvious that $T_\uparrow$ and $T_\downarrow$ are shifted to higher frequency as H_a increases. The reason is that the potential energy $V_0 = \hbar\gamma\mu_0 H_a$ rises with the increase of H_a. The influence of the EB field H_{eb} is shown in Figs. 3(e)–3(g), which can be interpreted by the decrease in the heights of barriers (and also the depths of wells) $\Delta V = \hbar\gamma\mu_0 H_{eb}$. On the one hand, for an up (down) state, the heights (depths) of the barriers (wells) decrease as H_{eb} decreases. Thus, $T_\uparrow$ ($T_\downarrow$) is shifted to lower (higher) frequency ranges; in other words, the TSSE become weaker. This result indicates that the TSSE is strongly dependent on the energy difference between the potential barriers and wells. On the other hand, ΔV also affects the strength of the scattering. It is the reason for the suppression of the oscillation amplitudes of $T_\uparrow$ and $T_\downarrow$.

As mentioned before, D is the key parameter for the MCMVs. It is found that the $D - \omega/2\pi$ curves are closely related to N, a, and b. We used a high-throughput screening method to find the MCMVs with high D and large bandwidth $\Delta\omega$ in various groups of (N, a, b). High D, which indicates a large on/off ratio, is necessary for the MCMVs. It is similar to the common interest in spin valves with higher GMR [41,42] or MTJs with larger TMR [43–49]. Thus, the critical transmission difference D_c is set for searching MCMVs with $D > D_c$ in the algorithm. Figure 4(a) is a screening example of the high-throughput screening at $D_c = 0.9$ and $\Delta\omega_c = 1$ GHz. $\Delta\omega_c$ represents the critical bandwidth and is also set for searching MCMVs with $\Delta\omega > \Delta\omega_c$ because large $\Delta\omega_c$ is also helpful for magnonic devices to achieve wide operating ranges. ω_c is the center operating frequency of the selected MCMVs. Figure 4(b) shows the pseudocode of the high-throughput algorithm. The screening steps are as follows. First, the $D - \omega/2\pi$ curves of various parameter groups (N, a, b) are calculated. Second, for each $D - \omega/2\pi$ curve, a continuous interval $\Delta\omega$ satisfying $D > D_c$ is sought out. Third, if $\Delta\omega > \Delta\omega_c$ is satisfied, (N, a, b) and ω_c are output as the parameters of the high-performance MCMVs.

Ultimately, 125 000 groups of (N, a, b) have been calculated. For $D_c = 0.9$ and $\Delta\omega_c = 1$ GHz, 1948 groups of (N, a, b) were screened out, as shown in Fig. 4(c). ω_c is distributed in the range of 20.4–51.4 GHz, as shown by the color bar. As D_c increases to 0.95, the number of (N, a, b) decreases to 1397 [Fig. 4(d)]. For $D_c = 0.95$ and $\Delta\omega_c = 1.5$ GHz, there are still 303 MCMVs [Fig. 4(e)]. Figure 4(f) shows the screening results at $D_c = -0.95$ and $\Delta\omega_c = 1.5$ GHz. The number of the extracted (N, a, b) is 61. Here, D_c is negative, suggesting that the up state is on and the down state is off for the magnon transmission, which is different from Figs. 4(c)–4(e). This tunability may provide more functionalities for fabricating new types of magnon valves.

IV. CONCLUSION

In summary, we constructed a one-dimensional MC with a periodic EB field. It was found that the up (down) state of the MC corresponds to the rectangular *N*-fold barriers (wells) for exchange-dominated spin waves. The broadband transmission spectra in up and down states were calculated. On the one hand, the numerical results showed the phenomena of the magnon resonant transmission. On the other hand, a TSSE was found to interpret the difference in the transmission spectra between the two states, which was also useful for designing the MCMVs. With the high-throughput screening method, 125 000 parameter-groups of MCs were calculated, and a number of them helpful for high-performance MCMVs were screened out. Our work theoretically investigated the exchange-dominated spin-wave transmission in rectangular *N*-fold barriers and wells and will also provide guidance for designing future magnonic devices.

ACKNOWLEDGMENTS

This work was supported by the National Key Research and Development Program of China (MOST, Grants No. 2017YFA0206200 and No. 2016YFA0300802), the National Natural Science Foundation of China (NSFC, Grants No. 51831012 and No. 51620105004), and the Beijing Natural Science Foundation (Grant No. Z201100004220006) and partially supported by the Strategic Priority Research Program (B) (Grant No. XDB33000000) of the Chinese Academy of Sciences (CAS).

[1] F. Bloch, Z. Phys. **61**, 206 (1930).
[2] T. Holstein and H. Primakoff, Phys. Rev. **58**, 1098 (1940).
[3] F. J. Dyson, Phys. Rev. **102**, 1217 (1956).
[4] V. V. Kruglyak and R. J. Hicken, J. Magn. Magn. Mater. **306**, 191 (2006).
[5] S. Neusser, B. Botters, and D. Grundler, Phys. Rev. B **78**, 054406 (2008).
[6] A. A. Serga, A. V. Chumak, and B. Hillebrands, J. Phys. D **43**, 264002 (2010).
[7] V. V. Kruglyak, S. O. Demokritov, and D. Grundler, J. Phys. D **43**, 264001 (2010).
[8] A. V. Chumak, V. I. Vasyuchka, A. A. Serga, and B. Hillebrands, Nat. Phys. **11**, 453 (2015).
[9] M. P. Kostylev, A. A. Serga, T. Schneider, B. Leven, and B. Hillebrands, Appl. Phys. Lett. **87**, 153501 (2005).
[10] T. Schneider, A. A. Serga, B. Leven, B. Hillebrands, R. L. Stamps, and M. P. Kostylev, Appl. Phys. Lett. **92**, 022505 (2008).
[11] S.-K. Kim, K.-S. Lee, and D.-S. Han, Appl. Phys. Lett. **95**, 082507 (2009).
[12] A. V. Chumak, A. A. Serga, and B. Hillebrands, Nat. Commun. **5**, 4700 (2014).
[13] H. Wu, L. Huang, C. Fang, B. S. Yang, C. H. Wan, G. Q. Yu, J. F. Feng, H. X. Wei, and X. F. Han, Phys. Rev. Lett. **120**, 097205 (2018).
[14] C. Y. Guo, C. H. Wan, X. Wang, C. Fang, P. Tang, W. J. Kong, M. K. Zhao, L. N. Jiang, B. S. Tao, G. Q. Yu, and X. F. Han, Phys. Rev. B **98**, 134426 (2018).
[15] Q. Wang, P. Pirro, R. Verba, A. Slavin, B. Hillebrands, and A. V. Chumak, Sci. Adv. **4**, e1701517 (2018).
[16] Q. Wang, T. Brächer, M. Mohseni, B. Hillebrands, V. I. Vasyuchka, A. V. Chumak, and P. Pirro, Appl. Phys. Lett. **115**, 092401 (2019).
[17] Z. Zhang, M. Vogel, J. Holanda, M. B. Jungfleisch, C. Liu, Y. Li, J. E. Pearson, R. Divan, W. Zhang, A. Hoffmann, Y. Nie, and V. Novosad, Appl. Phys. Lett. **115**, 232402 (2019).
[18] C. G. Sykes, J. D. Adam, and J. H. Collins, Appl. Phys. Lett. **29**, 388 (1976).
[19] A. V. Chumak, A. A. Serga, and B. Hillebrands, J. Phys. D **50**, 244001 (2017).
[20] S. A. Nikitov, P. Tailhades, and C. S. Tsai, J. Magn. Magn. Mater. **236**, 320 (2001).
[21] M. Krawczyk and D. Grundler, J. Phys.: Condens. Matter **26**, 123202 (2014).
[22] A. V. Chumak, A. A. Serga, B. Hillebrands, and M. P. Kostylev, Appl. Phys. Lett. **93**, 022508 (2008).
[23] A. V. Chumak, A. A. Serga, S. Wolff, B. Hillebrands, and M. P. Kostylev, Appl. Phys. Lett. **94**, 172511 (2009).
[24] M. Vogel, A. V. Chumak, E. H. Waller, T. Langner, V. I. Vasyuchka, B. Hillebrands, and G. von Freymann, Nat. Phys. **11**, 487 (2015).
[25] H. Yamamoto, Y. Kanie, H. Sano, and K. Taniguchi, Phys. Status Solidi B **169**, K17 (1992).
[26] C. L. Roy and A. Khan, Phys. Status Solidi B **176**, 101 (1993).
[27] G. N. Kakazei, P. E. Wigen, K. Y. Guslienko, V. Novosad, A. N. Slavin, V. O. Golub, N. A. Lesnik, and Y. Otani, Appl. Phys. Lett. **85**, 443 (2004).
[28] B. Lenk, H. Ulrichs, F. Garbs, and M. Münzenberg, Phys. Rep. **507**, 107 (2011).
[29] S.-J. Lee, J.-H. Moon, H.-W. Lee, and K.-J. Lee, Phys. Rev. B **96**, 184433 (2017).
[30] Z. Wang, Y. Cao, and P. Yan, Phys. Rev. B **100**, 064421 (2019).
[31] S. Ikeda, K. Miura, H. Yamamoto, K. Mizunuma, H. D. Gan, M. Endo, S. Kanai, J. Hayakawa, F. Matsukura, and H. Ohno, Nat. Mater. **9**, 721 (2010).
[32] P. Zilske, D. Graulich, M. Dunz, and M. Meinert, Appl. Phys. Lett. **110**, 192402 (2017).
[33] J. Cho, J. Jung, S.-Y. Cho, and C.-Y. You, J. Magn. Magn. Mater. **395**, 18 (2015).
[34] See Supplemental Material at http://link.aps.org/supplemental/10.1103/PhysRevB.103.054425 for more details in the corresponding section, which includes Refs. [29,30,37–39].
[35] P. Yan, X. S. Wang, and X. R. Wang, Phys. Rev. Lett. **107**, 177207 (2011).
[36] W. Wang, M. Albert, M. Beg, M.-A. Bisotti, D. Chernyshenko, D. Cortés-Ortuño, I. Hawke, and H. Fangohr, Phys. Rev. Lett. **114**, 087203 (2015).
[37] J. Lan, W. Yu, R. Wu, and J. Xiao, Phys. Rev. X **5**, 041049 (2015).
[38] W. Yu, J. Lan, R. Wu, and J. Xiao, Phys. Rev. B **94**, 140410(R) (2016).

[39] C. Jia, D. Ma, A. F. Schäffer, and J. Berakdar, Nat. Commun. **10**, 2077 (2019).
[40] W. J. Hsueh, C. H. Chen, and R. Z. Qiu, Phys. Lett. A **377**, 1378 (2013).
[41] M. N. Baibich, J. M. Broto, A. Fert, F. Nguyen Van Dau, F. Petroff, P. Etienne, G. Creuzet, A. Friederich, and J. Chazelas, Phys. Rev. Lett. **61**, 2472 (1988).
[42] G. Binasch, P. Grünberg, F. Saurenbach, and W. Zinn, Phys. Rev. B **39**, 4828(R) (1989).
[43] M. Julliere, Phys. Lett. A **54**, 225 (1975).
[44] T. Miyazaki and N. Tezuka, J. Magn. Magn. Mater. **139**, L231 (1995).
[45] J. S. Moodera, L. R. Kinder, T. M. Wong, and R. Meservey, Phys. Rev. Lett. **74**, 3273 (1995).
[46] H. X. Wei, Q. H. Qin, M. Ma, R. Sharif, and X. F. Han, J. Appl. Phys. **101**, 09B501 (2007).
[47] S. Yuasa, T. Nagahama, A. Fukushima, Y. Suzuki, and K. Ando, Nat. Mater. **3**, 868 (2004).
[48] S. S. P. Parkin, C. Kaiser, A. Panchula, P. M. Rice, B. Hughes, M. Samant, and S.-H. Yang, Nat. Mater. **3**, 862 (2004).
[49] Y. M. Lee, J. Hayakawa, S. Ikeda, F. Matsukura, and H. Ohno, Appl. Phys. Lett. **90**, 212507 (2007).
[50] Q. Qin, H. Lu, S. N. Zhu, C. S. Yuan, Y. Y. Zhu, and N. B. Ming, Appl. Phys. Lett. **82**, 4654 (2003).